materials

MDPI

Article

The New High-Pressure Phases of Nitrogen-Rich Ag–N Compounds

Ran Liu [1], Dan Xu [1], Zhen Yao [1,*], Shifeng Niu [1,2,*] and Bingbing Liu [1,*]

[1] State Key Laboratory of Superhard Materials, College of Physics, Jilin University, Changchun 130012, China; liuran@jlu.edu.cn (R.L.); xudan@jlu.edu.cn (D.X.)
[2] School of Physics and Engineering, Henan University of Science and Technology, Luoyang 471023, China
* Correspondence: yaozhen@jlu.edu.cn (Z.Y.); niusf19@mails.jlu.edu.cn (S.N.); liubb@jlu.edu.cn (B.L.)

Abstract: The high-pressure phase diagram of Ag–N compounds is enriched by proposing three stable high-pressure phases (P4/mmm-AgN_2, P1-AgN_7 and P-1-AgN_7) and two metastable high-pressure phases (P-1-AgN_4 and P-1-AgN_8). The novel N_7 rings and N_{20} rings are firstly found in the folded layer structure of P-1-AgN_7. The electronic structure properties of predicted five structures are studied by the calculations of the band structure and DOS. The analyses of ELF and Bader charge show that the strong N–N covalent bond interaction and the weak Ag–N ionic bond interaction constitute the stable mechanism of Ag–N compounds. The charge transfer between the Ag and N atoms plays an important role for the structural stability. Moreover, the P-1-AgN_7 and P-1-AgN_8 with the high-energy density and excellent detonation properties are potential candidates for new high-energy density species.

Keywords: polymeric nitrogen; high-energy density; high-pressure

Citation: Liu, R.; Xu, D.; Yao, Z.; Niu, S.; Liu, B. The New High-Pressure Phases of Nitrogen-Rich Ag–N Compounds. *Materials* **2022**, *15*, 4986. https://doi.org/10.3390/ma15144986

Academic Editor: Yurii Sharkeev

Received: 12 May 2022
Accepted: 15 July 2022
Published: 18 July 2022

1. Introduction

Due to the significant energy differences between the N–N bond, N=N bond and N≡N bond, polymeric nitrogen with the single/double bond structure is the potential high-energy-density materials (HEDMs). Moreover, the decomposition product of polymeric nitrogen is the clean diatomic nitrogen gas (N_2). Thus, the polymeric nitrogen can be used as the environmentally friendly HEDM. Many efforts have been performed for exploring the novel polymeric nitrogen structures, such as the chain-shaped structures (ch, Cmcm, PP) [1,2], the layered structures (A7, BP-N, LP-N, LB-N) [1,3–5], the caged structures (N_{10}) [6], the networked structures (cg-N, rcg-N, P-42$_1$m, P2$_1$2$_1$2$_1$, P2$_1$/m, C2/c, P2$_1$2$_1$2$_1$-500, Pnnm, P2$_1$, CW) [1,7–9] and the molecular crystal structures (N_2-N_6, N_6, N_8, 2N_5) [10–13]. Up to now, the cg-N, BP-N, LP-N and HLP-N have been successfully synthesized at (110 GPa, 2000 K), (146 GPa, 2200 K), (150 GPa, 3000 K) and (244 GPa, 3300 K), respectively. The study of decomposition shows that the cg-N, BP-N, LP-N and HLP-N can be quenched down to 42 GPa, 48 GPa, 52 GPa and 66 GPa, respectively [14–18]. Clearly, the harsh synthesis conditions (P > 100 GPa, T > 2000 K) and the low stability of polymeric nitrogen limit its application.

Recent studies show that introducing an impurity element (M) into the pure nitrogen structure can induce the novel polynitrogen structures, which may exhibit the excellent properties, such as the mild synthesis conditions, high stability, etc. A series of polynitrogen structures has been reported in theoretical studies. Typically, the novel N_4 ring is reported for P4/mmm-MnN_4, Cm-Al_2N_7, P-1-Na_2N_8, P2$_1$/c-Li_2N_4, C2/m-MgN_4 and Immm-AlN_4 compounds [19–22]. Especially, the regular N_4 rings results in a superhard property of P4/mmm-MnN_4 and Cm-Al_2N_7. The N_5 ring structures are found in the M_2N_5 (M = Na) and MN_5 (M = Li, Na, Rb, Cs, Ca, Sr, Ba, Cu) compounds [23–29]. More interestingly, the double-, triple- and quadruple-N_5 ring structures are found in MN_{10} (M = Be, Mg, Ba), MN_{15} (M = Al, Ga, Sc, Y) and HfN_{20} compounds, respectively [30–33]. Among these

reported structures, the $P2_1$-LiN_5, Cm-NaN_5, Pc-RbN_5 and P-1-BaN_{10} are stable with the pressure larger than 9.9 GPa, 20 GPa, 30 GPa and 12 GPa, respectively. The Fdd2-BeN_{10} and Fdd2-MgN_{10} compounds are possibly synthesized at relatively low pressures (around 28 GPa for BeN_{10} and 12 GPa for MgN_{10}) and can be preserved under ambient pressure. The good gravimetric energy density of Fdd2-BeN_{10} (5.39 kJ/g), Fdd2-MgN_{10} (3.48 kJ/g) and Cc-AlN_{15} (5.31 kJ/g) makes them the potential (HEDMs). The novel N_6 ring structures are found in MN_3 (M = Cs, Ca, Sr, K, Mg) [26–28,34–38] and MN_6 (M = W) compounds [39,40]. Among them, the P-1-MgN_3 phase with the N_6 ring structure is recoverable at ambient pressure [36]. The superhard R-3m-WN_6 remains dynamically stable at ambient conditions [40]. The N-chain structures are found in MN_4 (M = Be, Cd, Fe, Gd, Re, Os, W, Ru, Zn) [41–48], GdN_6 [45], ReN_8 [49] and HfN_{10} compounds [50]. Among them, P-1-BeN_4, γ-P-1-BeN_4 and δ-P-1-BeN_4 with the N-chain structures can be synthesized under pressures of 25.4, 20.8 and 27.4 GPa, respectively, which is greatly lower than 110 GPa for synthesizing the cg-N. The analysis of dynamical and thermal stability shows that the P-1-GdN_6 can be recovered to ambient conditions upon synthesis under compression. The Immm-HfN_{10} is discovered to be stable at moderate pressure above 23 GPa and can be preserved as a metastable phase at ambient pressure. The novel N_{18}-ring, N_6 + N_{10}-ring, N_{10}-ring and N_{18}-ring layered structures are found in P6/mcc-K_2N_{16}, C2/m-BaN_6, $P2_1$/c-BeN_4 and P-31c-CoN_8 compounds, respectively [31,51–53]. Moreover, the N_{14}-ring band-shape structure is the first reported for P-1-CoN_{10} [53]. The P-31c-CoN_8 (6.14 kJ/g) and P-1-CoN_{10} (5.18 kJ/g) with high-energy density can be quenched down to ambient conditions. The three-dimensional network structures are found in the C2/m-CdN_6, $I4_1$/a-HeN_4, R-3m-HeN_6, P63/m-HeN_{10} and C2/m-HeN_{22} [43,54,55]. The C2/m-CdN_6 and C2/m-HeN_{22} with respectively high-energy-density values of 3.82 kJ/g and 10.44 kJ/g may be quenchable to ambient pressure. In the experiment, the cyclo-N_5 ring in LiN_5, NaN_5 and CsN_5 compounds are synthesized at 45, 52 and 65 GPa, respectively [56–58]. The CsN_5 and LiN_5 can be quenched down to 18 GPa and ambient pressure, respectively. The armchair-like hexazine N_6 ring in R-3m-WN_6 is synthesized with pressure larger than 126 GPa [59]. The N-chain structure in Ibam-MgN_4 and FeN_4 are synthesized at 50 and 180 GPa, respectively [60,61]. As the review above, we know that the introduced impurity element can induce the novel polymeric nitrogen structures, which may exhibit more prominent properties than the pure polymeric nitrogen structures, such as the milder synthesis pressure and the higher stability.

Silver nitrides have received much attention for their outstanding chemical and physical properties, such as the energetic explosive, propulsion application, gas generators, photographic materials, etc. [62–64]. Recently, the armchair–antiarmchair N-chain and N_5 ring structures are severally reported for AgN_3 and AgN_5/AgN_6 compounds [65,66]. Beyond that, no other new silver nitrides with the high-pressure polymeric structures have been reported. Thus, a detailed high-pressure study that considers the different stoichiometry in silver nitrides is necessary for exploring new polynitrogen polymeric structures.

2. Computation Details

The structural research has been performed by the particle swarm optimization methodology implemented in the CALYPSO structure prediction method [67]. The structure optimizations and property calculations have been carried out by the Vienna ab initio simulation package (VASP) code [68]. The generalized gradient approximation (GGA) with the Perdew–Burke–Ernzerhof (PBE) exchange–correlation function has been employed for the first-principles calculations [69–71]. The $4d^{10}5s^1$ and $2s^22p^3$ are treated as the valence electrons of Ag and N atoms, respectively. In order to ensure that the enthalpy is converged to less than 1 meV/atom, the cutoff energy of Projector Augmented Wave (PAW) pseudopotential and the Monkhorst–Pack k-mesh density are severally set to 520 eV and $2\pi \times 0.03$ $Å^{-1}$ in the calculation. The ΔH^f of each Ag–N structure is calculated by using the following equation: ΔH^f (AgN_x) = [H(AgN_x) − H(AgN) − (x − 1) H(N)]/(1 + x). The most stable structures of AgN (Abma-phase) and N (P2/c- and cg-phases) are chosen as the reference structures in their corresponding stable pressure range. The phonon frequencies

have been calculated by using the finite displacement approach through the PHONOPY code [72]. The 2 × 2 × 2 supercell with the lattice size of about 10 Å is constructed in the calculation of phonon. The dissociation energies are calculated by considering the following decomposition paths: $AgN_x \rightarrow Ag + x/2N_2$. The $P6_3/mmc$ phase of Ag and Pa $\bar{3}$ phase of N_2 are the decomposition productions, respectively. The detonation velocity and detonation pressure have been calculated by using the Kamlet–Jacobs simi-empirical equation: $V_d = 1.01(NM^{0.5}E_d{}^{0.5})^{0.5}(1 + 1.30\rho)$ and $P_d = 15.58\rho^2NM^{0.5}E_d{}^{0.5}$. N represents the moles of gas per gram of AgNx, M represents the average molar mass of gas products, E_d is the detonation chemical energy, and ρ is the mass density.

3. Results and Discussion

Eight stoichiometries of AgN_x (x = 2, 3, 4, 5, 6, 7, 8, 10) are considered in the structural research with the simulation cells containing 1, 2 and 4 formula units (f.u.). The prediction for each stoichiometry is carried out at three pressures (50, 100 and 150 GPa). As shown in Figure 1a–c, the formation enthalpies (ΔH^f) of Ag–N compounds are presented in the thermodynamic convex hull. The solid squares on the convex hull are the thermodynamically stable phases, while the ones that deviate from the convex hull are the metastable/unstable phases. For the AgN_2 stoichiometry, we found the thermodynamically stable P4/mmm phase at 100 and 150 GPa. At 50 and 100 GPa, the reported P-1-AgN_3 in Ref. [65] is also found in this work. For the AgN_7 stoichiometry, the thermodynamically stable P1 and P-1 phases are found at 50 GPa and 100/150 GPa, respectively. No thermodynamically stable phases are found for the rest of the stoichiometries (AgN_4, AgN_5, AgN_6, AgN_8 and AgN_{10}). For the presented high-pressure phase diagrams of AgN_2 and AgN_7 in Figure 1d, we can see that the P4/mmm-AgN_2 is thermodynamically stable in the pressure region of (75–150 GPa). The P1-AgN_7 and P-1-AgN_7 are thermodynamically stable in the pressure ranges of (25–75 GPa) and (125–150 GPa), respectively. The dynamical stability of AgN_2 and AgN_7 are further evaluated by the phonon dispersion. As shown in Figure 2, no imaginary frequency is found throughout the Brillouin zone, indicating that the P4/mmm-AgN_2, P1-AgN_7 and P-1-AgN_7 are dynamically stable at 100, 50 and 150 GPa, respectively. Interestingly, the presented phonon dispersion curves in Figure 3 show that the P-1-AgN_4 and P-1-AgN_8 are dynamically stable at 150 GPa, indicating that they are the metastable phases. Moreover, the mechanical stabilities of P4/mmm-AgN_2, P1-AgN_7, P-1-AgN_7, P-1-AgN_4 and P-1-AgN_8 are evaluated by the calculation of elastic constants (Table 1). According to the mechanical stability criteria of tetragonal structure of ($C_{11} > |C_{12}|$, $2C_{13}{}^2 < C_{33}(C_{11} + C_{12})$, $C_{44} > 0$), we know that the tetragonal P4/mmm-AgN_2 is mechanically stable. The mechanical stability criteria of monoclinic structure are shown as follows [73]:

$$C_{11} > 0, C_{22} > 0, C_{33} > 0, C_{44} > 0, C_{55} > 0, C_{66} > 0, [C_{11} + C_{22} + C_{33} + 2(C_{12} + C_{13} + C_{23})] > 0,$$
$$C_{33}C_{55}\text{-}C_{35}{}^2 > 0, C_{44}C_{66}\text{-}C_{46}{}^2 > 0, C_{22} + C_{33}\text{-}2C_{23} > 0,$$
$$C_{22}(C_{33}C_{55}\text{-}C_{35}{}^2) + 2C_{23}C_{25}C_{35}\text{-}(C_{23}{}^2)C_{55}\text{-}(C_{25}{}^2)C_{33} > 0,$$
$$2[C_{15}C_{25}(C_{33}C_{12}\text{-}C_{13}C_{23}) + C_{15}C_{35}(C_{22}C_{13}\text{-}C_{12}C_{23}) + C_{25}C_{35}(C_{11}C_{23}\text{-}C_{12}C_{13})]\text{-}$$
$$[C_{15}{}^2(C_{22}C_{33}\text{-}C_{23}{}^2) + C_{25}C_{25}(C_{11}C_{33}\text{-}C_{13}{}^2) + C_{35}C_{35}(C_{11}C_{22}\text{-}C_{12}{}^2)] + C_{55}g > 0.$$

We can see that the elastic tensors Cij of P1-AgN_7, P-1-AgN_7, P-1-AgN_4 and P-1-AgN_8 satisfy the criteria, indicating that they possess the mechanical stability. Thus, we proposed three stable high-pressure phases (P4/mmm-AgN_2, P1-AgN_7 and P-1-AgN_7) and two metastable high-pressure phases (P-1-AgN_4 and P-1-AgN_8) by the structural prediction method.

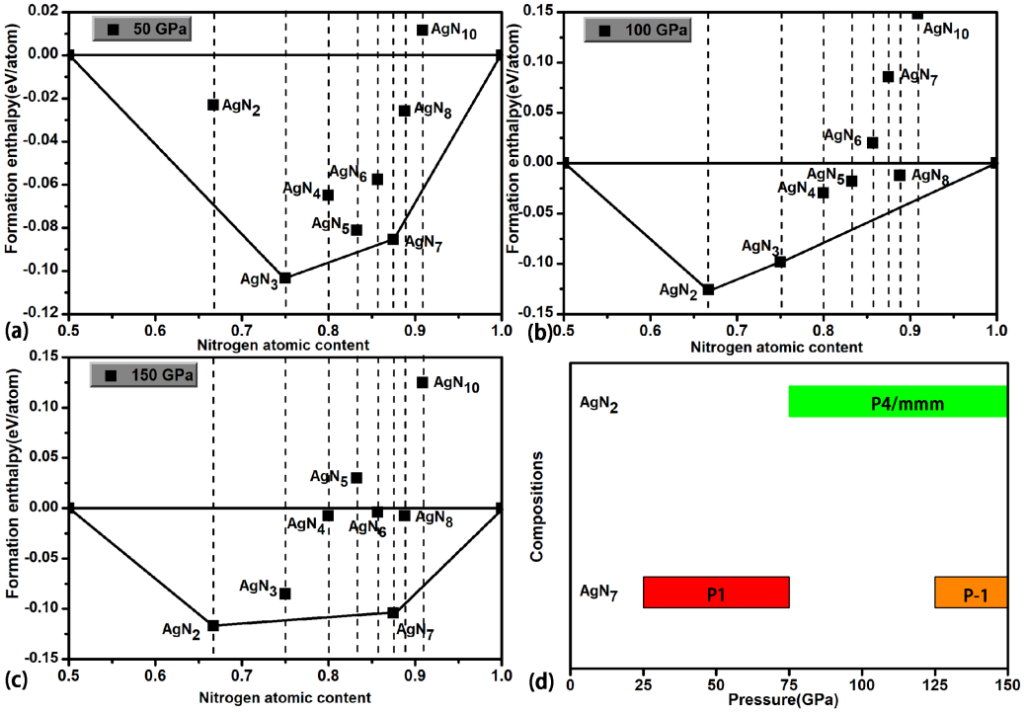

Figure 1. The formation enthalpies of Ag-N phases with respect to the Abma-AgN phase and nitrogen solids at different pressures (**a**–**c**). (**d**) shows the phase diagram of AgN_2 and AgN_7.

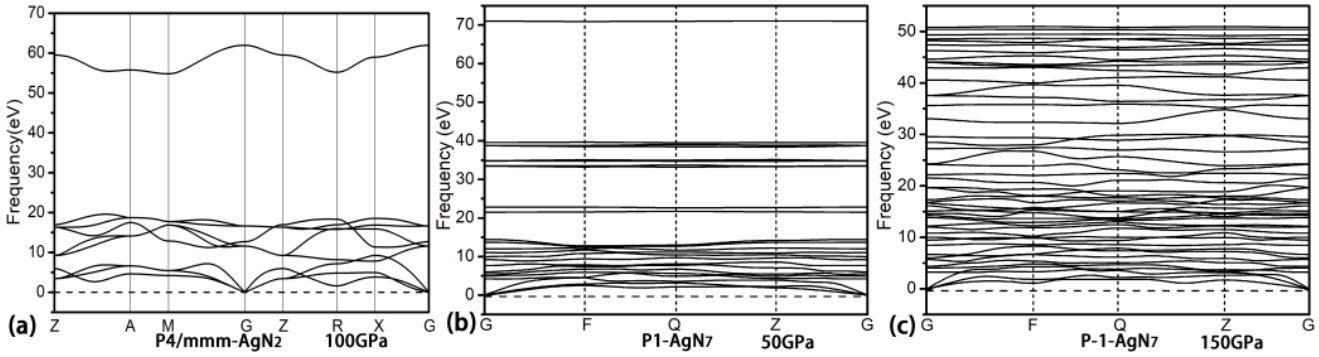

Figure 2. The phonon dispersion of P4/mmm-AgN_2 at 100 GPa (**a**), the P1-AgN_7 at 50 GPa (**b**) and P-1-AgN_7 at 150 GPa (**c**).

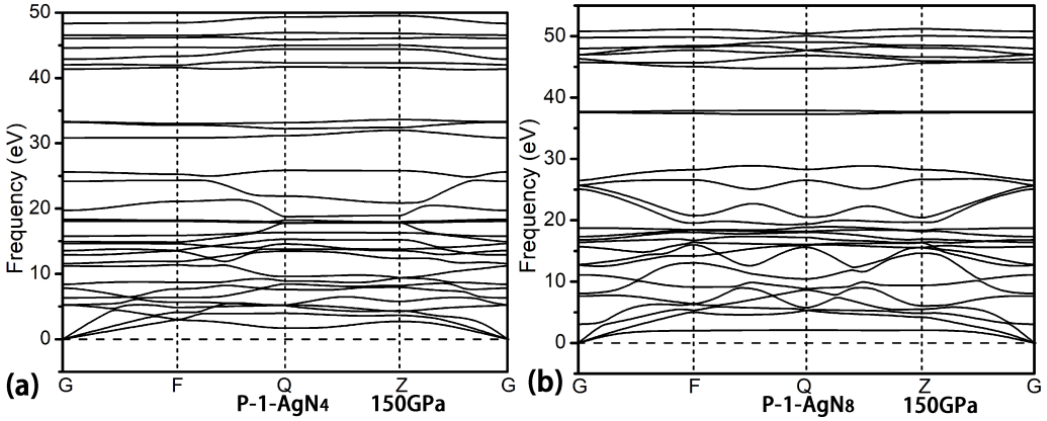

Figure 3. The phonon dispersion of P-1-AgN_4 at 150 GPa (**a**) and P-1-AgN_8 at 150 GPa (**b**).

Table 1. The elastic constants Cij (GPa) of the Ag–N compounds at high pressure.

AgN_x	(GPa)	C_{11}	C_{22}	C_{33}	C_{44}	C_{55}	C_{66}	C_{12}	C_{13}	C_{15}	C_{23}	C_{25}	C_{35}	C_{46}
P4/mmm-AgN_2	100	563	-	648	85	-	22	313	310	-	-	-	-	-
P1-AgN_7	50	215	294	231	70	68	42	160	154	−3	173	−5	8	24
P-1-AgN_7	150	943	942	800	221	207	279	513	396	−85	377	−113	−19	−85
P-1-AgN_4	150	910	912	710	127	148	270	593	354	−42	338	−39	49	27
P-1-AgN_8	150	1163	1114	861	193	56	250	604	152	−17	228	−24	12	0.24

The crystal structures of P4/mmm-AgN_2, P1-AgN_7, P-1-AgN_7, P-1-AgN_4 and P-1-AgN_8 are presented in Figure 4. In P4/mmm-AgN_2, the polymeric N-structure unit is the dumbbell-shaped N_2 structure, which is composed of two equivalent nitrogen atoms. At 100 GPa, the bond length of N_1-N_1 is 1.165 Å. For the P1-AgN_7 presented in Figure 4b, one unit cell contains one dumbbell-shaped N_2 structure and one N_5 ring structure. The N_5 ring structure is composed of five inequitable nitrogen atoms (N_1->N_5), while the dumbbell-shaped N_2 structure is composed of two inequitable nitrogen atoms (N_6-N_7). At 50 GPa, the bond lengths of N_1-N_5, N_2-N_3, N_3-N_4, N_4-N_5, N_5-N_1 and N_6-N_7 are 1.296 Å, 1.309 Å, 1.296 Å, 1.301 Å, 1.307 Å and 1.114 Å, respectively. The P-1-AgN_7 is the folded layer structure, which is constituted by the N_{20} ring and two fused N_7 rings. At 150 GPa, the bond lengths of ten N–N bonds (N_1-N_4, N_4-N_3, N_3-N_2, N_2-N_2, N_2-N_5, N_5-N_6, N_6-N_1, N_6-N_6, N_4-N_7 and N_7-N_7) that are constructed by seven inequitable nitrogen atoms (N_1->N_7) are 1.286 Å, 1.315 Å, 1.270 Å, 1.286 Å, 1.274 Å, 1.282 Å, 1.254 Å, 1.318 Å, 1.277 Å and 1.261 Å, respectively. Up to now, the reported N-rings in the polynitrogen structures are the N_5, N_6, N_{10}, N_{12}, N_{14} and N_{18} rings [51–54]. As the construction unit of the layer structure, the novel N_7 rings and N_{20} rings are firstly reported for this work. The P-1-AgN_4 is the 1-D chain structure, which is constructed by the alternate N_2 and N_6 ring. At 150 GPa, the bond lengths of five N–N bonds (N_1-N_1, N_1-N_2, N_2-N_3, N_3-N_4 and N_4-N_2) that are constructed by four inequitable nitrogen atoms (N_1->N_4) are 1.266 Å, 1.282 Å, 1.300 Å, 1.281 Å and 1.306 Å, respectively. The P-1-AgN_8 is the layer structure, which is constructed by the fused N_{18} ring structure. At 150 GPa, the bond lengths of five N–N bonds (N_1-N_4, N_4-N_4, N_1-N_2, N_2-N_2 and N_1-N_3,) that are constructed by four inequitable nitrogen atoms (N_1->N_4) are 1.271 Å, 1.257 Å, 1.272 Å, 1.269 Å and 1.280 Å, respectively.

The electronic structural properties including the band structure, the density of states (DOS), the electronic local function (ELF) and the Bader charge transfer are calculated for analyzing the electronic structure property and stable mechanism of structures. As shown in Figure 5, the P4/mmm-AgN_2 at 100 GPa and P1-AgN_7 at 50 GPa are the semiconductor phases with the band gaps of 1.0 eV and 2.4 eV, respectively. For the P4/mmm-AgN_2, the electronic states of valence bands near the Fermi level are mainly contributed by the Ag_d and N_p orbitals, while the conduction bands near the Fermi level are mainly contributed by the Ag_s and N_p orbitals. For the P1-AgN_7, the electronic states of valence bands near the Fermi level are mainly contributed by the Ag_d and N_p orbitals, while the conduction bands near the Fermi level are mainly contributed by the N_p orbitals. The P-1-AgN_7 at 150 GPa is the metal phase, for which the electronic states near the Fermi level are mainly contributed by the N_p orbitals. For the presented band structure and DOS in Figure 6, the P-1-AgN_4 and P-1-AgN_8 at 150 GPa are both the metal phases, for which the electronic states of valence bands near the Fermi level are mainly contributed by the Ag_d and N_p orbitals, while the conduction bands near the Fermi level are mainly contributed by the N_p orbitals.

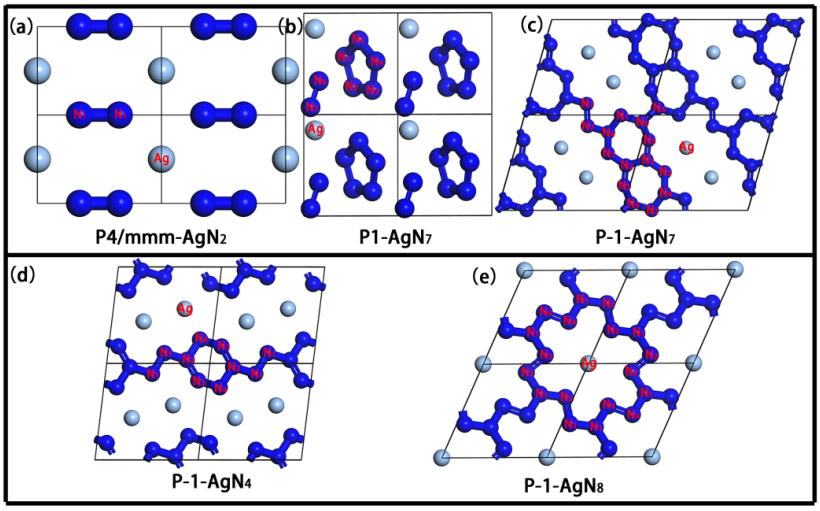

Figure 4. The 2 × 2 × 2 supercell structures of Ag-N compounds: P4/mmm-AgN_2 (**a**), P1-AgN_7 (**b**), P-1-AgN_7 (**c**), P-1-AgN_4 (**d**) and P-1-AgN_8 (**e**).

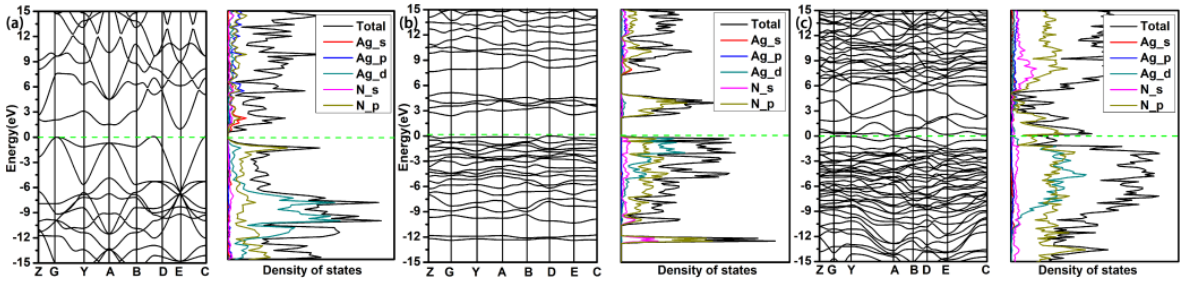

Figure 5. Band structures and projected density of states of P4/mmm-AgN_2 at 100 GPa (**a**), P1-AgN_7 at 50 GPa (**b**), P-1-AgN_7 at 150 GPa (**c**).

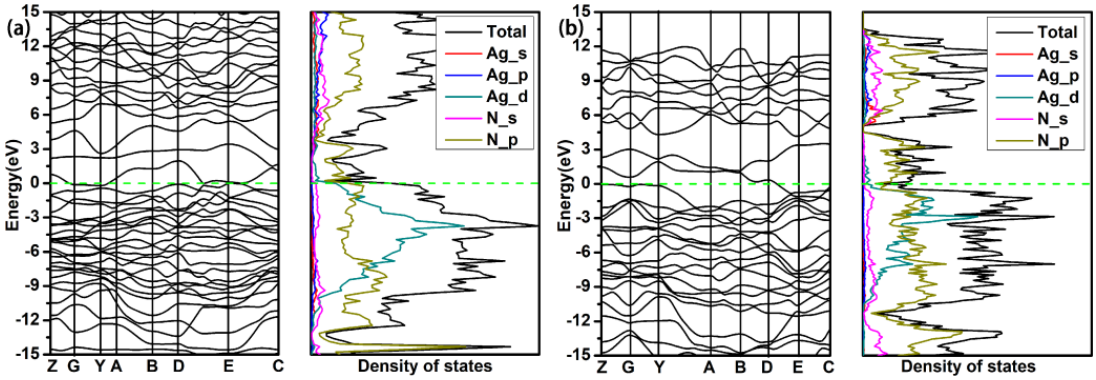

Figure 6. Band structures and projected density of states of P-1-AgN_4 (**a**) and P-1-AgN_8 (**b**) at 150 GPa.

In Figure 7, as the fixed value of isovalue (0.8) in ELF, the high localization electronic states between the nitrogen atoms indicate the strong N–N covalent bond interaction. The lone electron pairs distribute at the outside corner of N atoms for reducing the repulsive interaction. In combination with the analysis of Figure 4, we know that the N atom in the dumbbell-shaped N_2 structure of P4/mmm-AgN_2 and P1-AgN_7 hybridizes in the sp state, which is formed by one N–N σ bond and one lone pair electron. The N atom in the N_5 ring hybridizes in the sp^2 state, which is formed by two N–N σ bonds and one lone electron pair. In the P-1-AgN_7, the N_1, N_3, N_5 and N_7 atoms hybridize in sp^2 states, which are formed by two N–N σ bonds and one lone electron pair, while the N_2, N_4, and N_6 atoms hybridize in sp^3 states, which are formed by three N–N σ bonds and one lone electron

pair. In the P $\bar{1}$-AgN_4, the N_1, N_3, and N_4 atoms hybridize in sp^2 states, which are formed by two N–N σ bonds and one lone electron pair, while the N_2 atom hybridizes in the sp^3 state, which is formed by three N–N σ bonds and one lone electron pair. In the P $\bar{1}$-AgN_8, the N_2, N_3, and N_4 atoms hybridize in sp^2 states, which are formed by two N–N σ bonds and one lone electron pair, while the N_1 atom hybridizes in the sp^3 state, which is formed by three N–N σ bonds and one lone electron pair. No localization electron is distributed around the Ag atom and between the Ag and N atoms due to the weak Ag–N electronic overlap interaction. As the presented charge transfer in Table 2, we can see that the Ag and N atoms are severally the electron donor and receptor, which means the weak Ag–N ionic bond interaction. Clearly, this charge transfer enhances the N–N covalent bond and Ag–N ionic bond interaction, which improves the structural stability. According to the above discussion, we know that the stable mechanism of our predicted Ag–N compounds originates from the strong N–N covalent bond interaction and the weak Ag–N ionic bond interaction. Moreover, the charge transfer between the Ag and N atoms plays an important part in their structural stability.

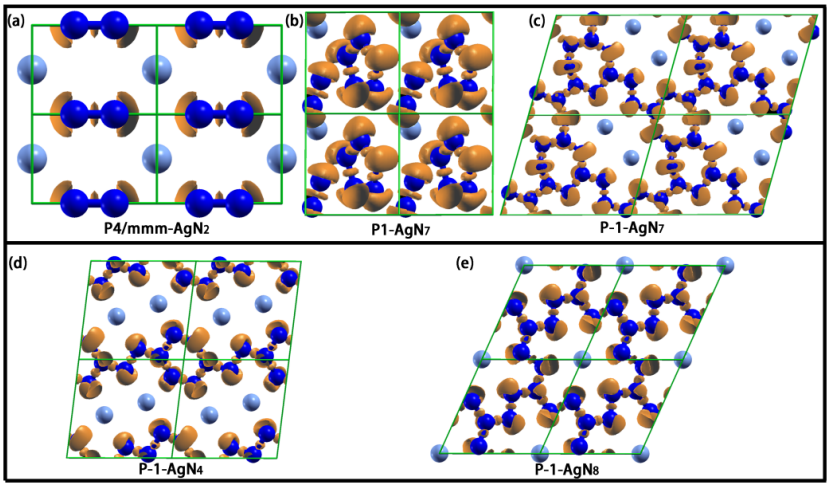

Figure 7. The ELFs of P4/mmm-AgN_2 (**a**), P1-AgN_7 (**b**), P-1-AgN_7 (**c**), P-1-AgN_4 (**d**) and P-1-AgN_8 (**e**) (isovalue = 0.8).

Table 2. The Bader charge analysis of P4/mmm-AgN_2, P1-AgN_7, P-1-AgN_7, P-1-AgN_4 and P-1-AgN_8 at different pressures. The negative and positive values mean the donor and the receptor of charge, respectively.

Structures	Pressure	Element	σ(e)/Atom
P4/mmm-AgN_2	100	Ag	−0.70
		N	+0.35
P1-AgN_7	50	Ag	−0.82
		N	+0.117
P-1-AgN_7	150	Ag	−0.623
		N	+0.089
P-1-AgN_4	150	Ag	−0.64
		N	+0.16
P-1-AgN_8	150	Ag	−0.76
		N	0.095

The energy densities and detonation properties of P-1-AgN_7 and P-1-AgN_8 are presented in Table 3. It can be seen that the energy density of P-1-AgN_7 and P-1-AgN_8 is

3.9 kJ/g, which is close to that of the TNT (4.3 kJ/g). The detonation velocities of P-1-AgN_7 (13.58 km/s) and P-1-AgN_8 (17.59 km/s) are 2.0 and 2.5 times the value (6.90 km/s) of TNT, respectively. The detonation pressures of P-1-AgN_7 (115.5 GPa) and P-1-AgN_8 (210.7 GPa) are 6 and 11 times the value (19.00 GPa) of TNT. Thus, the P-1-AgN_7 and P-1-AgN_8 are potential candidates for new high-energy density species.

Table 3. The energy density and detonation properties of P-1-AgN_7 and P-1-AgN_8 compounds in comparison to TNT.

Compounds	Energy Densities (kJ/g)	Detonation Velocity (km/s)	Detonation Pressure (GPa)
P-1-AgN_7	3.90	13.58	115.5
P-1-AgN_8	3.90	17.59	210.7
TNT	4.30	6.90	19.00

4. Conclusions

The crystal structure, electronic structure and energy property of silver nitrides in nitrogen-rich aspects are studied by using the first-principles calculations combining the particle-swarm structural searching. In addition to the reported P-1-AgN_3, three stable high-pressure phases (P4/mmm-AgN_2, P1-AgN_7 and P-1-AgN_7) and two metastable high-pressure phases (P-1-AgN_4 and P-1-AgN_8) are proposed by the structural prediction method. The stable pressure range of P4/mmm-AgN_2, P1-AgN_7 and P-1-AgN_7 are proposed by the enthalpy difference analysis. Interestingly, the novel N_7 rings and N_{20} rings are firstly found in the folded layer structure of P-1-AgN_7. In electronic structure analysis, the P4/mmm-AgN_2 and P1-AgN_7 are the semiconductor phases, while the P-1-AgN_7, P-1-AgN_4 and P-1-AgN_8 are the metal phases. The analysis of ELF and Bader charge shows that the stable mechanism of predicted Ag–N compounds originates from the strong N–N covalent bond interaction and the weak Ag–N ionic bond interaction. Moreover, the charge transfer between the Ag and N atoms plays an important role for their structural stability. The P-1-AgN_7 and P-1-AgN_8 with the high energy densities and excellent detonation properties are potential candidates for new high-energy density species. This work not only enriched the high-pressure phase diagram of Ag–N compounds but also proposed two new high-energy density structures.

Author Contributions: Conceptualization, Z.Y. and B.L.; methodology, S.N. and D.X.; software, S.N.; investigation, R.L., D.X. and S.N.; data curation, R.L. and S.N.; writing—original draft preparation, R.L., Z.Y. and S.N.; writing—review and editing, R.L., S.N. and Z.Y.; project administration and funding acquisition, B.L. All authors have read and agreed to the published version of the manuscript.

Funding: This work was financially supported by the National Key R&D Program of China (No. 2018YFA0305900 and 2018YFA0703404) and the National Natural Science Foundation of China under Grant No 11634004, 51320105007, 11604116 and 51602124, and the Program for Changjiang Scholars and Innovative Research Team in University of Ministry of Education of China under Grant No IRT1132.

Institutional Review Board Statement: Not applicable.

Informed Consent Statement: Not applicable.

Data Availability Statement: The data presented in this study are available on request from the corresponding author.

Conflicts of Interest: The authors declare no conflict of interest.

References

1. Wang, X.L.; Tian, F.B.; Wang, L.C.; Cui, T.; Liu, B.B.; Zou, G.T. Structural stability of polymeric nitrogen: A first-principles investigation. *J. Chem. Phys.* **2010**, *132*, 024502. [CrossRef] [PubMed]

2. Wang, X.L.; He, Z.; Ma, Y.M.; Cui, T.; Liu, Z.M.; Liu, B.B.; Li, J.F.; Zou, G.T. Prediction of a new layered phase of nitrogen from first-principles simulations. *J. Phys. Condens. Matter.* **2007**, *19*, 425226. [CrossRef]
3. Alemany, M.M.G.; Martins, J.L. Density-functional study of nonmolecular phases of nitrogen: Metastable phase at low pressure. *Phys. Rev. B* **2003**, *68*, 024110. [CrossRef]
4. Ma, Y.M.; Oganov, A.R.; Li, Z.W.; Yu, X.; Kotakoski, J. Novel high pressure structures of polymeric nitrogen. *Phys. Rev. Lett.* **2009**, *102*, 065501. [CrossRef] [PubMed]
5. Zahariev, F.; Hu, A.; Hooper, J.; Zhang, F.; Woo, T. Layered single-bonded nonmolecular phase of nitrogen from first-principles simulation. *Phys. Rev. B* **2005**, *72*, 214108. [CrossRef]
6. Wang, X.L.; Wang, Y.C.; Miao, M.S.; Zhong, X.; Lv, J.; Cui, T.; Li, J.F.; Chen, L.; Pickard, C.J.; Ma, Y.M. Cagelike diamondoid nitrogen at high pressures. *Phys. Rev. Lett.* **2012**, *109*, 175502. [CrossRef] [PubMed]
7. Pickard, C.J.; Needs, R.J. High-pressure phases of nitrogen. *Phys. Rev. Lett.* **2009**, *102*, 125702. [CrossRef]
8. Sun, M.; Yin, Y.Y.; Pang, Z.K. Predicted new structures of polymeric nitrogen under 100–600 GPa. *Comput. Mater. Sci.* **2015**, *98*, 399–404. [CrossRef]
9. Zahariev, F.; Hooper, J.; Alavi, S.; Zhang, F.; Woo, T.K. Low-pressure metastable phase of single-bonded polymeric nitrogen from a helical structure motif and first-principles calculations. *Phys. Rev. B* **2007**, *75*, 140101. [CrossRef]
10. Mattson, W.D.; Sanchez-Portal, D.; Chiesa, S.; Martin, R.M. Prediction of new phases of nitrogen at high pressure from first-principles simulations. *Phys. Rev. Lett.* **2004**, *93*, 125501. [CrossRef]
11. Greschner, M.J.; Zhang, M.; Majumdar, A.; Liu, H.Y.; Peng, F.; Tse, J.S.; Yao, Y.S. A New Allotrope of Nitrogen as High-Energy Density Material. *J. Phys. Chem. A* **2016**, *120*, 2920–2925. [CrossRef] [PubMed]
12. Hirshberg, B.; Gerber, R.B.; Krylov, A.I. Calculations predict a stable molecular crystal of N_8. *Nat. Chem.* **2014**, *6*, 52–56. [CrossRef] [PubMed]
13. Liang, D.M.; Liu, H.Y.; Gan, Y.D.; Kuang, A.; Tian, C.L. A novel low-pressure structure of polymeric nitrogen. *Chin. Sci. Bull.* **2021**, *66*, 2908–2914. [CrossRef]
14. Eremets, M.I.; Gavriliuk, A.G.; Trojan, I.A.; Dzivenko, D.A.; Boehler, R. Single-bonded cubic form of nitrogen. *Nat. Mater.* **2004**, *3*, 558–563. [CrossRef] [PubMed]
15. Tomasino, D.; Kim, M.; Smith, J.; Yoo, C.S. Pressure-induced symmetry-lowering transition in dense nitrogen to layered polymeric nitrogen (LP-N) with colossal Raman intensity. *Phys. Rev. Lett.* **2014**, *113*, 205502. [CrossRef]
16. Laniel, D.; Geneste, G.; Weck, G.; Mezouar, M.; Loubeyre, P. Hexagonal Layered Polymeric Nitrogen Phase Synthesized near 250 GPa. *Phys. Rev. Lett.* **2019**, *122*, 066001. [CrossRef]
17. Ji, C.; Adeleke, A.A.; Yang, L.X.; Wang, B.; Gou, H.Y.; Yao, Y.S.; Li, B.; Meng, Y.; Smith, J.S.; Prakapenda, V.B.; et al. Nitrogen in black phosphorus structure. *Sci. Adv.* **2020**, *6*, edba9206. [CrossRef]
18. Laniel, D.; Winkler, B.; Fedotenko, T.; Pakhomova, A.; Chariton, S.; Milman, V.; Prakapenka, V.; Dubrovinsky, L.; Dubrovinskaia, N. High-Pressure Polymeric Nitrogen Allotrope with the Black Phosphorus Structure. *Phys. Rev. Lett.* **2020**, *124*, 216001. [CrossRef]
19. Niu, S.; Xu, D.; Li, H.Y.; Yao, Z.; Liu, S.; Zhai, C.G.; Hu, K.; Shi, X.H.; Wang, P.; Liu, B.B. Pressure-stabilized polymerization of nitrogen in manganese nitrides at ambient and high pressures. *Phys. Chem. Chem. Phys.* **2022**, *24*, 5738–5747. [CrossRef]
20. Du, H.F.; Ge, Y.F.; Zhu, J.L.; Guo, W.; Yao, Y.G. Pressure-induced novel nitrogen-rich aluminum nitrides: AlN_6, Al_2N_7 and AlN_7 with polymeric nitrogen chains and rings. *Phys. Chem. Chem. Phys.* **2021**, *23*, 12350–12359. [CrossRef]
21. Bondarchuk, S.V. Recoverability of N_4^{x-} Anions to Ambient Pressure: A First Principles Study of cyclo- and syn-Tetranitrogen Units. *J. Phys. Chem. C* **2021**, *125*, 7368–7377. [CrossRef]
22. Li, L.; Bao, K.; Zhao, X.B.; Cui, T. Bonding Properties of Manganese Nitrides at High Pressure and the Discovery of MnN_4 with Planar N_4 Rings. *J. Phys. Chem. C* **2021**, *125*, 24605–24612. [CrossRef]
23. Peng, F.; Yao, Y.S.; Liu, H.Y.; Ma, Y.M. Crystalline LiN_5 Predicted from First Principles as a Possible High-Energy Material. *J. Phys. Chem. Lett.* **2015**, *6*, 2363–2366. [CrossRef] [PubMed]
24. Steele, B.A.; Oleynik, I.I. Sodium pentazolate: A nitrogen rich high energy density material. *Chem. Phys. Lett.* **2016**, *643*, 21–26. [CrossRef]
25. Williams, A.S.; Steele, B.A.; Oleynik, I.I. Novel rubidium poly-nitrogen materials at high pressure. *J. Chem. Phys.* **2017**, *147*, 234701. [CrossRef]
26. Peng, F.; Han, Y.X.; Liu, H.Y.; Yao, Y.S. Exotic stable cesium polynitrides at high pressure. *Sci. Rep.* **2015**, *5*, 16902. [CrossRef]
27. Zhu, S.S.; Peng, F.; Liu, H.Y.; Majumdar, A.; Gao, T.; Yao, Y.S. Stable Calcium Nitrides at Ambient and High Pressures. *Inorg. Chem.* **2016**, *55*, 7550–7555. [CrossRef]
28. Wei, S.L.; Liu, Y.; Li, D.; Liu, Z.; Wang, W.J.; Tian, F.B.; Bao, K.; Duan, D.F.; Liu, B.B.; Cui, T. Pressure-Stabilized Polymerization of Nitrogen in Alkaline-Earth Metal Strontium Nitrides. *Phys. Chem. Chem. Phys.* **2020**, *22*, 5242. [CrossRef]
29. Li, J.F.; Sun, L.; Wang, X.L.; Zhu, H.Y.; Miao, M.S. Simple Route to Metal cyclo-N_5–Salt: High-Pressure Synthesis of CuN_5. *J. Chem. Phys. C* **2018**, *122*, 22339–22344. [CrossRef]
30. Xia, K.; Zheng, X.X.; Yuan, J.N.; Liu, C.; Gao, H.; Wu, Q.; Sun, J. Pressure-Stabilized High-Energy-Density Alkaline-Earth-Metal Pentazolate Salts. *J. Phys. Chem. C* **2019**, *123*, 10205–10211. [CrossRef]
31. Huang, B.W.; Frapper, G. Barium–Nitrogen Phases under Pressure: Emergence of Structural Diversity and Nitrogen-Rich Compound. *Chem. Mater.* **2018**, *30*, 7623–7636. [CrossRef]

32. Xia, K.; Yuan, J.N.; Zheng, X.X.; Liu, C.; Gao, H.; Wu, Q.; Sun, J. Predictions on High-Power Trivalent Metal Pentazolate Salts. *J. Phys. Chem. Lett.* **2019**, *10*, 6166–6173. [CrossRef] [PubMed]
33. Huang, B.W.; Wang, B.S.; Wu, S.H.; Guégan, F.; Hu, W.Y.; Frapper, G. Predicted Polymeric and Layered Covalent Networks in Transition Metal Pentazolate M(cyclo-N_5)$_x$ Phases at Ambient and High Pressure: Up to 20 Nitrogen Atoms per Metal. *Chem. Mater.* **2021**, *33*, 5298–5307. [CrossRef]
34. Zhang, M.G.; Yan, H.Y.; Wei, Q.; Liu, H.Y. A new high-pressure polymeric nitrogen phase in potassium azide. *RSC Adv.* **2015**, *5*, 11825–11830. [CrossRef]
35. Zhang, J.; Zeng, Z.; Lin, H.Q.; Li, Y.L. Pressure-induced planar N_6 rings in potassium azide. *Sci. Rep.* **2014**, *4*, 4358. [CrossRef] [PubMed]
36. Yu, S.Y.; Huang, B.W.; Zeng, Q.F.; Oganov, A.R.; Zhang, L.T.; Frapper, G. Emergence of Novel Polynitrogen Molecule-like Species, Covalent Chains, and Layers in Magnesium–Nitrogen Mg_xN_y Phases under High Pressure. *J. Phys. Chem. C* **2017**, *121*, 11037–11046. [CrossRef]
37. Wei, S.L.; Li, D.; Liu, Z.; Li, X.; Tian, F.B.; Duan, D.F.; Liu, B.B.; Cui, T. Alkaline earth metal (Mg) polynitrides at high pressure as possible high-energy materials. *Phys. Chem. Chem. Phys.* **2017**, *19*, 9246–9252. [CrossRef] [PubMed]
38. Hou, P.G.; Lian, L.L.; Cai, Y.M.; Liu, B.; Wang, B.; Wei, S.L.; Li, D. Structural phase transition and bonding properties of high-pressure polymeric CaN_3. *RSC Adv.* **2018**, *8*, 4314–4320. [CrossRef]
39. Li, Q.; Sha, L.; Zhu, C.; Yao, Y.S. New multifunctional tungsten nitride with energetic N_6 and extreme hardness predicted from first principles. *EPL* **2017**, *118*, 46001. [CrossRef]
40. Xia, K.; Gao, H.; Liu, C.; Yuan, J.N.; Sun, J.; Wang, H.-T.; Xing, D.Y. A novel superhard tungsten nitride predicted by machine-learning accelerated crystal structure search. *Sci. Bull.* **2018**, *63*, 817–824. [CrossRef]
41. Zhang, S.T.; Zhao, Z.Y.; Liu, L.L.; Yang, G.C. Pressure-induced stable BeN_4 as a high energy density material. *J. Power Sources* **2017**, *365*, 155–161. [CrossRef]
42. Zhang, X.J.; Xie, X.; Dong, H.F.; Zhang, X.; Wu, F.G.; Mu, Z.F.; Wen, M.R. Pressure-Induced High-Energy-Density BeN_4 Materials with Nitrogen Chains: First Principles Study. *J. Phys. Chem. C* **2021**, *125*, 25376–25382. [CrossRef]
43. Niu, S.; Li, Z.H.; Li, H.Y.; Shi, X.H.; Yao, Z.; Liu, B.B. New Cadmium-Nitrogen Compounds at High Pressures. *Inorg. Chem.* **2021**, *60*, 6772–6781. [CrossRef] [PubMed]
44. Wu, L.L.; Tian, R.F.; Wan, B.; Liu, H.Y.; Gong, N.; Chen, P.; Shen, T.; Yao, Y.S.; Gou, H.Y.; Gao, F. Prediction of Stable Iron Nitrides at Ambient and High Pressures with Progressive Formation of New Polynitrogen Species. *Chem. Mater.* **2018**, *30*, 8476–8485. [CrossRef]
45. Liu, L.L.; Wang, D.H.; Zhang, S.T.; Zhang, H.J. Pressure-stabilized GdN_6 with an armchair–antiarmchair structure as a high energy density material. *J. Mater. Chem. A* **2021**, *9*, 16751–16758. [CrossRef]
46. Aydin, S.; Ciftci, Y.O.; Tatar, A. Superhard transition metal tetranitrides: XN_4(X. = Re, Os, W). *J. Mater. Res.* **2012**, *27*, 1705–1715. [CrossRef]
47. Zhang, Y.K.; Wu, L.L.; Wan, B.; Lin, Y.Z.; Hu, Q.Y.; Zhao, Y.; Gao, R.; Li, Z.P.; Zhang, J.W.; Gou, H.Y. Diverse ruthenium nitrides stabilized under pressure: A theoretical prediction. *Sci. Rep.* **2016**, *6*, 33506. [CrossRef]
48. Shi, X.H.; Yao, Z.; Liu, B.B. New High-Pressure Phases of the Zn–N System. *J. Phys. Chem. C* **2020**, *124*, 4044–4049. [CrossRef]
49. Wu, L.L.; Zhou, P.Y.; Li, Y.G.; Wan, B.; Sun, S.H.; Xu, J.J.; Sun, J.; Liao, B.; Gou, H.Y. Ultra-incompressibility and high energy density of ReN_8 with infinite nitrogen chains. *J. Mater. Sci.* **2020**, *56*, 3814–3826. [CrossRef]
50. Zhang, J.; Oganov, A.R.; Li, X.F.; Niu, H.Y. Pressure-stabilized hafnium nitrides and their properties. *Phys. Rev. B* **2017**, *95*, 020103. [CrossRef]
51. Steele, B.A.; Oleynik, I.I. Novel Potassium Polynitrides at High Pressures. *J. Phys. Chem. A* **2017**, *121*, 8955–8961. [CrossRef]
52. Wei, S.L.; Li, D.; Liu, Z.; Wang, W.J.; Tian, F.B.; Bao, K.; Duan, D.F.; Liu, B.B.; Cui, T. A Novel Polymerization of Nitrogen in Beryllium Tetranitride at High Pressure. *J. Phys. Chem. C* **2017**, *121*, 9766–9772. [CrossRef]
53. Liu, S.; Liu, R.; Li, H.Y.; Yao, Z.; Shi, X.H.; Wang, P.; Liu, B.B. Cobalt-Nitrogen Compounds at High Pressure. *Inorg. Chem.* **2021**, *60*, 14022–14030. [CrossRef] [PubMed]
54. Li, Y.W.; Feng, X.L.; Liu, H.Y.; Hao, J.; Redfern, S.A.T.; Lei, W.W.; Liu, D.; Ma, Y.M. Route to high-energy density polymeric nitrogen t-N via He-N compounds. *Nat. Commun.* **2018**, *9*, 722. [CrossRef] [PubMed]
55. Hou, J.Y.; Weng, X.-J.; Oganov, A.R.; Shao, X.; Gao, G.Y.; Dong, X.; Wang, H.-T.; Tian, Y.J.; Zhou, X.-F. Helium-nitrogen mixtures at high pressure. *Phys. Rev. B* **2021**, *103*, L060102. [CrossRef]
56. Laniel, D.; Weck, G.; Gaiffe, G.; Garbarino, G.; Loubeyre, P. High-Pressure Synthesized Lithium Pentazolate Compound Metastable under Ambient Conditions. *J. Phys. Chem. Lett.* **2018**, *9*, 1600–1604. [CrossRef]
57. Bykov, M.; Bykova, E.; Chariton, S.; Prakapenka, V.B.; Batyrev, I.G.; Mahmood, M.F.; Goncharov, A.F. Stabilization of pentazolate anions in the high-pressure compounds Na_2N_5 and NaN_5 and in the sodium pentazolate framework $NaN_5 \bullet N_2$. *Dalton. Trans.* **2021**, *50*, 7229–7237. [CrossRef]
58. Steele, B.A.; Stavrou, E.; Crowhurst, J.C.; Zaug, J.M.; Prakapenka, V.B.; Oleynik, I.I. High-Pressure Synthesis of a Pentazolate Salt. *Chem. Mater.* **2017**, *29*, 735–741. [CrossRef]
59. Salke, N.P.; Xia, K.; Fu, S.Y.; Zhang, Y.J.; Greenberg, E.; Prakapenka, V.B.; Liu, J.; Sun, J.; Lin, J.F. Tungsten Hexanitride with Single-Bonded Armchairlike Hexazine Structure at High Pressure. *Phys. Rev. Lett.* **2021**, *126*, 065702. [CrossRef]

60. Bykov, M.; Khandarkhaeva, S.; Fedotenko, T.; Sedmak, P.; Dubrovinskaia, N.; Dubrovinsky, L. Synthesis of FeN_4 at 180 GPa and its crystal structure from a submicron-sized grain. *Acta. Cryst.* **2018**, *74*, 1392–1395.
61. Laniel, D.; Winkler, B.; Koemets, E.; Fedotenko, T.; Bykov, M.; Bykova, E.; Dubrovinsky, L.; Dubrovinskaia, N. Synthesis of magnesium-nitrogen salts of polynitrogen anions. *Nat. Commun.* **2019**, *10*, 4515. [CrossRef] [PubMed]
62. Hou, D.B.; Zhang, F.X.; Ji, C.; Hannon, T.; Zhu, H.Y.; Wu, J.Z.; Levitas, V.I.; Ma, Y.Z. Phase transition and structure of silver azide at high pressure. *J. Appl. Phys.* **2011**, *110*, 023524. [CrossRef]
63. Li, D.M.; Zhu, P.F.; Wang, Y.J.; Liu, B.B.; Jiang, J.R.; Huang, X.L.; Wang, X.L.; Zhu, H.Y.; Cui, Q.L. High-pressure spectroscopic study of silver azide. *RSC Adv.* **2016**, *6*, 82270–82276. [CrossRef]
64. Zhu, W.H.; Xiao, H.M. First-principles study of structural and vibrational properties of crystalline silver azide under high pressure. *J. Solid-State Chem.* **2007**, *180*, 3521–3528. [CrossRef]
65. Niu, S.F.; Liu, R.; Shi, X.H.; Yao, Z.; Liu, B.B.; Lu, S.C. High-pressure new phase of AgN_3. *Mod. Phys. Lett. B* **2021**, *35*, 2150386. [CrossRef]
66. Williams, A.S.; Cong, K.N.; Gonzalez, J.M.; Oleynik, I.I. Crystal structure of silver pentazolates AgN_5 and AgN_6. *Dalton Trans.* **2021**, *50*, 16364. [CrossRef]
67. Wang, Y.C.; Lv, J.; Zhu, L.; Ma, Y.M. CLYPSO: A method for crystal structure prediction. *Comput. Phys. Commun.* **2012**, *183*, 2063–2070. [CrossRef]
68. Kresse, G. Furthmüller, Efficient iterative schemes for ab initio total-energy calculating using a plane-wave basis set. *Phys. Rev. B* **1996**, *54*, 11169–11186. [CrossRef]
69. Monkhorst, H.J.; Pack, J.D. Special points for Brillouin-zone integrations. *Phys. Rev. B* **1976**, *13*, 5188–5192. [CrossRef]
70. Hohenberg, P.; Kohn, W. Inhomogeneous electron gas. *Phys. Rev.* **1964**, *136*, B864–B871. [CrossRef]
71. Kohn, W.; Sham, L.J. Self-consistent equations including exchange and correlation effects. *Phys. Rev.* **1965**, *140*, A1133–A1138. [CrossRef]
72. Perdew, J.P.; Ruzsinszky, A.; Csonka, G.I.; Vydrov, O.A.; Scuseria, G.E.; Constantin, L.A.; Zhou, X.L.; Burke, K. Restoring the Density-Gradient Exxpansion for Exchange in Solids and Surfaces. *Phys. Rev. Lett.* **2008**, *100*, 136406. [CrossRef] [PubMed]
73. Wu, Z.J.; Zhao, E.J.; Xiang, H.P.; Hao, X.F.; Liu, X.J.; Meng, J. Crystal structures and elastic properties of superhard IrN_2 and IrN_3 from first principles. *Phys. Rev. B* **2007**, *76*, 054115. [CrossRef]